J Nanopart Res (2019) 21:71
https://doi.org/10.1007/s11051-019-4512-7

RESEARCH PAPER

Improved small-angle x-ray scattering of nanoparticle self-assembly using a cell with a flat liquid surface

Jiayang Hu · Evan W. C. Spotte-Smith · Brady Pan · Irving P. Herman

Received: 10 January 2019 / Accepted: 15 March 2019

Abstract One important way of forming nanostructures entails the assembly of nanoparticle (NP) monolayers at a liquid surface. Probing this assembly of 11.8-nm-diameter iron oxide NPs by small-angle x-ray scattering (SAXS) is studied using cells with walls at angles designed to significantly reduce the size of the meniscus. This enables the collection of much larger signals in the SAXS images of ordered arrays of NPs at liquid/gas interfaces, as is needed for kinetics studies and x-ray exposure minimization, along with the observation of extremely high degrees of order. Meniscus flattening and improved signal collection are demonstrated for the assembly of ordered arrays of iron oxide NP monolayers at a diethylene glycol surface.

Keywords Nanoparticle self-assembly · SAXS · GISAXS · Liquid surface · Meniscus · Nanoparticle monolayers

Introduction

The self-assembly of ordered arrays of nanoparticles (NPs) at liquid surfaces and interfaces, followed by transfer to a solid substrate, is one important way of forming nanostructures containing NPs (Grzelczak et al. 2010). Synchrotron small-angle x-ray scattering (SAXS) is often used to probe the formation of such NP monolayer arrays, both during and after their self-assembly (Boal et al. 2000; Böker et al. 2007; Narayanan et al. 2004). However, surface curvature due to the meniscus of the liquid on the cell walls (Adamson 1967) leads to complications in the SAXS interrogation of liquid interfaces that are not present when probing planar solid interfaces. We show how to improve such SAXS analysis, largely by flattening the liquid meniscus and avoiding these complications.

Curvature in the interrogated interface is expected to lead to smaller signals (1) due to the more limited interaction length of the collimated x-ray path with the surface or interfacial region and (2) when there is an increased x-ray path in a more strongly absorbing fluid (such as before and after the probed central region of the concave-up meniscus at the liquid surface in Fig. 1a), particularly when the height of the x-ray beam is much smaller than that of the meniscus. For, say an ordered two-dimensional (2D) array of NPs at a liquid surface, with improved NP order there are more orders of linear streaks in the SAXS pattern. Curvature does not change the number of orders that could be observed for a well-ordered NP array, but it (1) makes the streaks curved (Narayanan et al. 2004) and broadens them even when the x-ray beam hits the bottom of the meniscus (if the beam is not very narrow) and (2) could alter NP self-assembly interactions and so could also be a source of streak broadening.

The scattering cell design used here to investigate iron oxide NP monolayer assembly on the diethylene glycol (DEG) liquid surface has wall angles that match

J. Hu · E. W. C. Spotte-Smith · B. Pan · I. P. Herman (✉)
Department of Applied Physics and Applied Mathematics, Columbia University, New York, NY 10027, USA
e-mail: iph1@columbia.edu

Published online: 29 March 2019

the contact angle between a cell window and a liquid/gas interface, as seen in Fig. 1b. This lessens the curvature at the surface and consequently potentially lessens these deleterious features. It is seen that use of this cell significantly reduces the size of the meniscus, and this greatly increases the collected signal in the SAXS analysis of ordered NPs, which is important for the short exposures needed for kinetics studies (Josten et al. 2017; Narayanan et al. 2004; Weidman et al. 2016), and also lessens the need to use large x-ray exposures, which is known to damage NP structures (Lu et al. 2012) and likely NP ligands. This approach also enables the observation of extremely high degrees of order. Designing cell walls to achieve flat liquid-liquid interfaces has been used to study molecular layers with SAXS (Luo et al. 2006; Zhang et al. 1999).

Experimental procedure

SAXS measurements were made of self-assembled iron oxide NP arrays at the DEG surface in sample cells fabricated with three different types of central sections (bodies). Liquids and NP colloids were injected into each cell, and synchrotron SAXS measurements were made in them at the 11-BM beamline at the Brookhaven National Laboratory National Synchrotron Light Source II (NSLS-II). The x-ray windows on the entrance and exit sides of each cell body were 0.0762-mm-thick flat fluorinated ethylene propylene (FEP) because of their very small x-ray absorption. These bodies and the entrance and exit side flanges were made of the same type of material, each with O-ring grooves and screw holes. O-rings held the windows in place on either side and formed the inner seals after the bolts spanning from flange to body to flange were tightened (Fig. 1c).

The body design of the sample cell used in previous work on NP self-assembly on liquid surfaces (Zhang et al. 2015, 2016), called the "cylindrical cell," had a right circular cylinder (21.0-mm diameter, with 7.7-mm length) bored through aluminum, so the sidewalls were curved, and the x-ray windows were both vertical; small holes on the top and sides permitted fluid injection and evaporation of any volatile solvent.

Two different sample cells were manufactured using a Formlabs Form 2® printer, with a resin of methacrylic acid esters and photoinitiators to produce translucent or white poly(methyl methacrylate) (PMMA) when exposed to ultraviolet light. In the "tapered cell," the dimension of the cavity in the body along the x-ray path (the length) was 8.8 mm and the transverse dimension (the width) was 51.8 mm at the bottom (Fig. 1c). The entrance and exit walls, sealed by 57.7 mm × 22.8 mm FEP windows, and the sidewalls were all tapered outward from the bottom of the cell at an angle of 75° to the horizontal, so the length of the inner part of the body increased from 8.8 to 20.6 mm at the top, 22 mm above the bottom. This angle was chosen to match and thereby cancel the contact angle of DEG on FEP, as determined by dropping DEG on it and observing the angle formed between the liquid and solid surfaces; the same angle was used for the sidewalls to lessen the meniscus there. However, for the sidewalls, the 75° angle was used only halfway up (11-mm height, where the width had increased from 51.8 to 57.7 mm) and then the walls were vertical to the top (Fig. 1c). When used for SAXS, the cell was filled with DEG to a height of 5.5 mm to form a liquid substrate, so tapering was not needed all the way to the top.

The body of the second type of printed cells had vertical walls. The lengths and widths of the "reference printed cell" matched the corresponding values at the top of the liquid substrate in the tapered cell, 11.7 mm and 54.7 mm. Both printed cells had a square hole on top (Fig. 1c) that permitted solvent injection and evaporation. In other applications, a solid plug or one with a small hole can be inserted in this hole to control the escape of volatile solvent. The surface tension contact angle of DEG on FEP was the same for pure DEG, and for DEG that had sat in translucent or white PMMA tapered cells for 20 h under nitrogen, so (for the purpose of these experiments) use of PMMA did not affect the DEG and the meniscus formed.

Each cell was partially filled with DEG (with 1.3 mL (to 10.5-mm height) in the cylindrical cell, with 3.0 mL in the reference (4.7 mm) and tapered (5.5 mm) printed cells) to serve as a liquid substrate, and then a small amount of NP colloids in the highly volatile solvent hexane was drop-cast. DEG was chosen because it satisfies the needs of drop-casting, such as low volatility and insolubility with the hexane solvent (Zhang et al. 2015, 2016), and has a relatively low, though non-negligible, x-ray absorption coefficient of 164.54/m at the 13.5-keV photon energy used (Henke et al. 1993).

The formation of ordered 2D NP arrays in these cells was studied after drop-casting 20 μL of a colloid of iron oxide NPs in hexane (which contained the number of NPs needed to form one monolayer in that particular

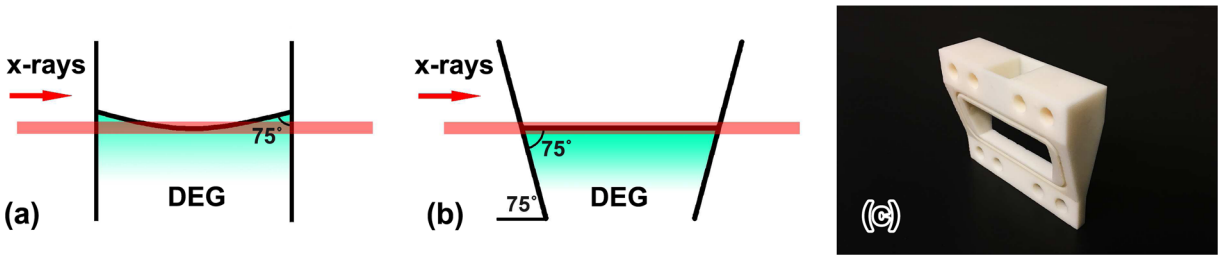

Fig. 1 Schematic of the x-ray path across cells with **a** vertical walls and a prominent meniscus and **b** walls at an angle to make the surface flat, in a tapered cell. **c** The body of the printed tapered cell before assembly. The white PMMA cell body is shown for clarity. The meniscus in **a** shows it is concave up for DEG. As seen in Fig. 2a and b, the meniscus heights are over 0.3 mm and 0.4 mm for the cylindrical and reference cells; the vertical size of the x-ray beam is smaller, 0.05 mm

cell) on top of the DEG substrate and subsequent hexane evaporation. This corresponded to an initial hexane thickness of 0.12 mm in the cylindrical cell and 0.03 mm in the printed cells (with these thicknesses assuming flat interfaces). NPs with a diameter of 11.8 nm were synthesized using previously published methods and subsequently encapsulated by oleate ligands (Hyeon et al. 2001). After rapid hexane evaporation (< 1 min in the printed cells), the structure of the NP monolayer at the liquid-gas surface was probed using SAXS. The x-ray beam size was 50 μm (vertical) × 200 μm (horizontal). The detector used for SAXS measurements was a Pilatus3 S 2M, which was set 3 m away from the sample cell. Before and after each SAXS measurement, the DEG meniscus was characterized by x-ray transmission as a function of vertical position.

Results and discussion

Figure 2 shows the x-ray transmission across the three cells filled with DEG (before the NP colloid in hexane was added) as a function of probing height, obtained by using a vertically moving stage. The intensity of the transmitted beam changes with the path length in the DEG at different heights due to the meniscus. The gradual changes in transmission in the (a) cylindrical and (b) reference cells (over 0.3 mm and 0.4 mm, respectively) at the surface indicate that the meniscus is very prominent. In contrast, the abrupt decrease in transmission in Fig. 2c (over 0.05 mm) shows that the meniscus has largely been removed in the tapered cell and that the surface of the DEG is nearly flat as expected. The transmission below the meniscus is larger in the cylindrical cell (~ 25%) than in the vertical wall cell (~ 12%) because its DEG path length is smaller. The gradual increase in signal in the tapered cell below the meniscus is due to the progressively shorter path length of absorbing DEG. X-ray transmission was the same after the NP colloid was added and SAXS was measured.

Figure 3 shows SAXS patterns from the well-ordered, close-packed hexagonal monolayer of iron oxide NPs on DEG in the three cells after the hexane had dried. The 1D intensity plots vs. the normal wavevector (plotted along the q_y axis, with each point integrated

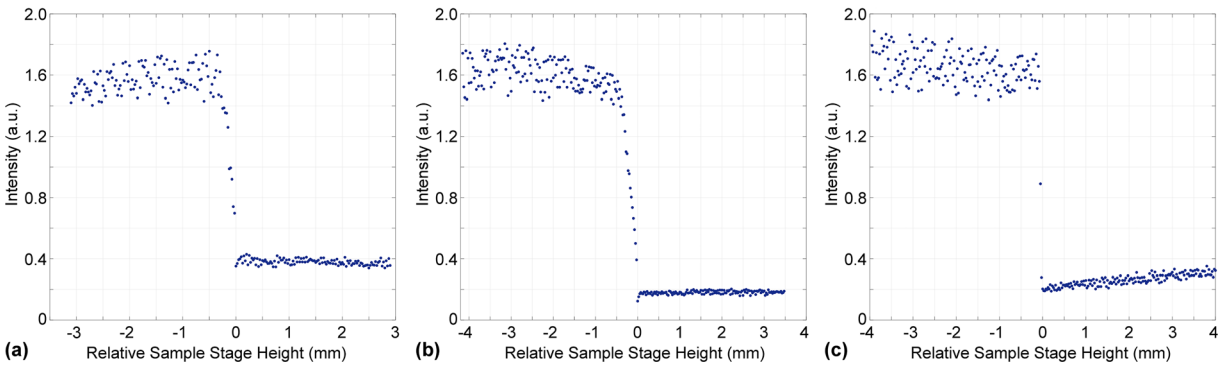

Fig. 2 Transmission of x-rays vs. height (relative to the measured bottom of each meniscus) for the **a** cylindrical cell, **b** reference translucent printed cell with vertical walls, and **c** tapered translucent printed cell, with data points every 0.025 mm

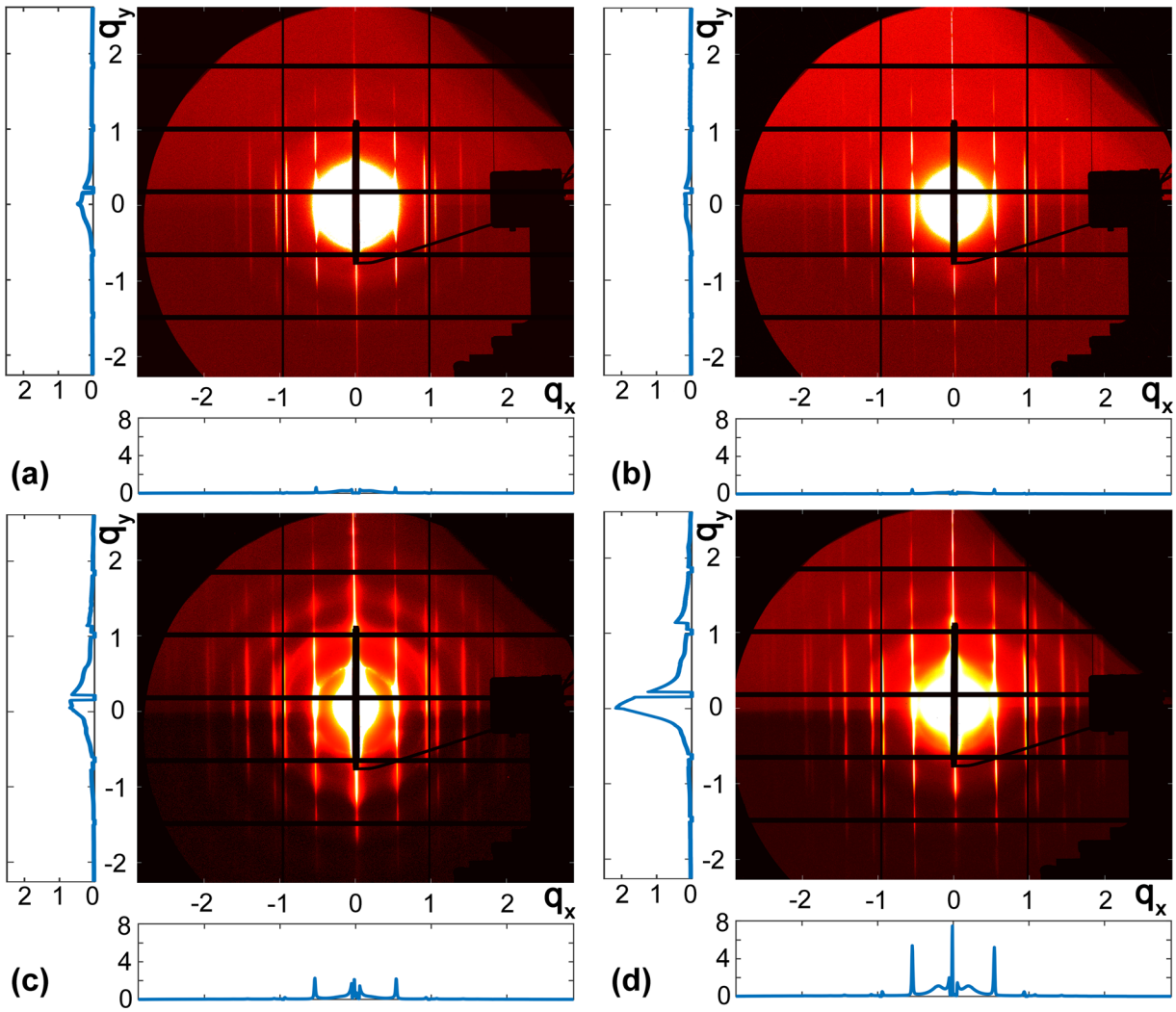

Fig. 3 SAXS images from a monolayer of iron oxide NPs on DEG, after hexane evaporation in the **a** cylindrical cell (7.7-mm path length, data collected over 120 s), **b** reference translucent printed cell (11.7 mm, 120 s), **c** tapered translucent printed cell (11.7 mm, 120 s), and **d** tapered white printed cell (11.7 mm, 150 s). The color scales for each image are set for maximum contrast. The 1D intensity traces vs. the normal and parallel wavevectors are also given for each image, plotted along the q_y and q_x axes, respectively, with those for **d** normalized to 120 s. All the wavevectors q are in nm^{-1} and intensities in millions of counts

over the full range of q_x in the image) and parallel wavevector (plotted along the q_x axis, with each point integrated over the full range of q_y in the image) are also given for each image, with the signals in Fig. 3d normalized to 120 s. In the cells with vertical walls, there are 5 orders or streaks on each side (4 are strong, 1 is weak) in the cylindrical cell (Fig. 3a) and 6 orders (4 strong, 2 weak) in the reference cell (Fig. 3b). In contrast, there are much stronger signals and several more visible orders, for a total of 8 orders (7 strong, 1 weak), in the translucent tapered cell (Fig. 3c). This observation shows the expected advantage of probing flatter liquid surfaces in cells with the tapered design. For reference, Fig. 3d shows very strong SAXS patterns, with 10 orders (7 strong, 3 weak), in the white tapered cell that were taken during an earlier visit to NSLS-II. (A thinner 0.0254-mm FEP window had been used in that earlier run; it was not used in the later ones because it bowed and led to cell leakage.) Differences in these last two images were likely due to uncontrolled variables, such as slight differences in the quality of the NP monolayer, relative x-ray beam position, and liquid surface flatness due to defects on the windows (for example, scratches (Pershan and Schlossman 2012)), and not the slightly

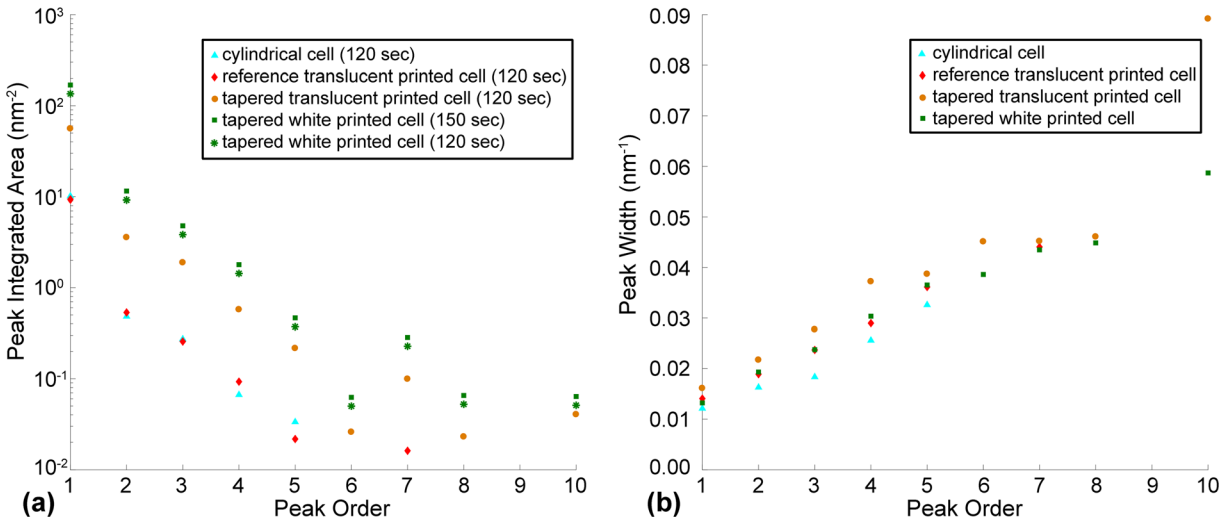

Fig. 4 Streak **a** integrated areas and **b** widths for the SAXS images in Fig. 3 for each cell, including area data for the tapered white printed cell with its 150-s-long run, and these areas normalized to the 120-s run duration used with the other cells. The widths in **b** are the full widths at half maximum for Gaussian fits

longer integration time for the latter image or differences in FEP window thickness or PMMA color.

These SAXS profile streaks were integrated along q_y from 0 to 0.253 nm^{-1} and then fit from $q_x = 0$ to -2.67 nm^{-1} to Gaussian profiles atop linear backgrounds. Streak areas for the 150-s-long acquisition times used with the white tapered cell are also plotted normalized to the 120-s times for the other three measurements. Only the pixels with positive q_y were measured, because their paths were in air while those for negative q_y were weaker due to the larger x-ray absorption in DEG, and only those with negative q_x were analyzed, because the beam stopper holder blocked a part of the image for positive q_x. Figure 4a shows that the SAXS streaks have much larger integrated areas, at least ~ 6–8× for corresponding orders, in the tapered translucent cell than in the other cells. The shorter x-ray path length in the cylindrical cell (7.7 mm) than in the tapered cells (11.7 mm, which is also the length for the untapered reference) could account for only a small part of this difference. The 6th and the 9th order peaks are weaker (near $q_y = 0$) than expected, because the SAXS pattern is the product of the form and structure factors, and these peaks have form factor minima near $q_y = 0$.

The widths of these fits are plotted in Fig. 4b. They are about the same in the tapered and untapered reference cells for corresponding orders, suggesting that the curvature in the probed region affects the width a little. They increase linearly with order as expected (Williamson and Hall 1953). However, they are both a bit larger for corresponding orders in the untapered aluminum cell, perhaps because in that cell a much shorter length was being probed and the region may have been more homogeneous.

FEP windows were used for each cell here, instead of the 0.0254-mm-thick Kapton windows used with the cylindrical cell in some earlier work (Zhang et al. 2015, 2016), because FEP has a larger contact angle with DEG; its smaller meniscus requires less tapering correction.

The meniscus is less prominent in the shorter cylindrical cell (Fig. 2a) than in the longer reference printed cell (Fig. 2b). This may be counter-intuitive, but is as expected from theory (Brennen 2006), as is the measured difference in meniscus height of ~ 0.1 mm. However, it is not advisable to make use of this trend and develop very short untapered cells, because the meniscus effect would remain significant and the interaction lengths would be very short.

Conclusions

Much larger SAXS signals and many more SAXS orders are observed for ordered monolayers on a liquid surface when a tapered cell is used that flattens the liquid surface. In future studies of NP assembly, the cell angles, dimensions, and materials can be varied to improve SAXS analysis further. We have focused on the menisci at the FEP windows, because they affect the SAXS

measurements the most, but cell design could also minimize the meniscus at the sidewalls and that at the corners, where the meniscus is the largest. Cells can also be designed and used to minimize the meniscus of a particular liquid/liquid interface to study NP assembly at that buried liquid interface.

Acknowledgments This research used the CMS 11-BM beamline and other resources of the National Synchrotron Light Source II (NSLS-II) and resources of the Center for Functional Nanomaterials, which are U.S. Department of Energy (DOE) Office of Science user facilities operated for the DOE Office of Science by Brookhaven National Laboratory (BNL) under Contract No. DE-SC0012704. We thank Drs. Masafumi Fukuto, Ruipeng Li, and Kevin Yager at the BNL NSLS-II CMS 11-BM beamline for their assistance, and Dr. Oleg Gang, Jason Cardarelli (IGERT program of the National Science Foundation (DGE-1069240)) and Roy Garcia.

Funding information Support was provided by the National Science Foundation (CBET-1603043).

Compliance with ethical standards

Conflict of interest The authors declare that they have no conflict of interest.

References

Adamson AW (1967) Physical chemistry of surfaces. Wiley-Interscience, New York

Boal AK, Ilhan F, DeRouchey JE, Thurn-Albrecht T, Russell TP, Rotello VM (2000) Self-assembly of nanoparticles into structured spherical and network aggregates. Nature 404:746–748

Böker A, He J, Emrick T, Russell TP (2007) Self-assembly of nanoparticles at interfaces. Soft Matter 3:1231–1248

Brennen CE (2006) An internet book on fluid dynamics. http://brennen.caltech.edu/fluidbook/. Accessed 12 April 2018

Grzelczak M, Vermant J, Furst EM, Liz-Marzan LM (2010) Directed self-assembly of nanoparticles. ACS Nano 4: 3591–3605

Henke BL, Gullikson EM, Davis JC (1993) Filter transmission. Lawrence Berkeley national laboratory. http://henke.lbl.gov/optical_constants/filter2.html. Accessed 30 Mar 2018

Hyeon T, Lee SS, Park J, Chung Y, Na HB (2001) Synthesis of highly crystalline and monodisperse maghemite nanocrystallites without a size-selection process. J Am Chem Soc 123:12798–12801

Josten E, Wetterskog E, Glavic A, Boesecke P, Feoktystov A, Brauweiler-Reuters E, Rücker U, Salazar-Alvarez G, Brückel T, Bergström L (2017) Superlattice growth and rearrangement during evaporation-induced nanoparticle self-assembly. Sci Rep 7:2802

Lu C, Akey AJ, Herman IP (2012) Synchrotron x-ray modification of nanoparticle superlattice formation. Appl Phys Lett 101: 133109

Luo G, Malkova S, Yoon J, Schultz DG, Lin B, Meron M, Benjamin I, Vanýsek P, Schlossman ML (2006) Ion distributions near a liquid-liquid interface. Science 311:216–218

Narayanan S, Wang J, Lin XM (2004) Dynamical self-assembly of nanocrystal superlattices during colloidal droplet evaporation by in situ small angle x-ray scattering. Phys Rev Lett 93: 135503

Pershan PS, Schlossman M (2012) Liquid surfaces and interfaces: synchrotron x-ray methods. Cambridge University Press, New York

Weidman MC, Smilgies DM, Tisdale WA (2016) Kinetics of the self-assembly of nanocrystal superlattices measured by real-time in situ x-ray scattering. Nat Mater 15:775–781

Williamson GK, Hall WH (1953) X-ray line broadening from filed aluminium and wolfram. Acta Metall 1:22–31

Zhang Z, Mitrinovic DM, Williams SM, Huang Z, Schlossman ML (1999) X-ray scattering from monolayers of $F(CF_2)_{10}(CH_2)_2OH$ at the water–(hexane solution) and water–vapor interfaces. J Chem Phys 110:7421–7432

Zhang D, Lu C, Hu J, Lee SW, Ye F, Herman IP (2015) Small angle x-ray scattering of iron oxide nanoparticle monolayers formed on a liquid surface. J Phys Chem C 119:10727–10733

Zhang D, Hu J, Kennedy KM, Herman IP (2016) Forming nanoparticle monolayers at liquid–air interfaces by using miscible liquids. Langmuir 32:8467–8472